AIAA AVIATION Forum
August 2-6, 2021, VIRTUAL EVENT
AIAA AVIATION 2021 FORUM

10.2514/6.2021-2493

Effect of Shock Wave Boundary Layer Interaction on Vibratory Response of a Compliant Panel

Marc A. Eitner* and Yoo-Jin Ahn† and Mustafa N. Musta ‡ and Leon Vanstone § and Jayant Sirohi ¶ and Noel T. Clemens‖

Department of Aerospace Engineering and Engineering Mechanics, The University of Texas at Austin, Austin, TX, 78712, USA

Flight vehicles that operate in the supersonic regime can be subject to adverse fluid-structure interactions due to their lightweight design. The presence of geometric obstructions such as control surfaces or fins can induce compression shocks that can interact with the boundary layer, leading to flow separation. The interaction of flow, compression shock and structural dynamics is very difficult to model and currently only poorly understood. This work investigates experimentally the interaction between a compliant panel in a Mach 2 flow under a ramp-induced shock wave boundary layer interaction (SWBLI). Brass panels of length 4.8'' and width 2.5'' and different thicknesses (h=0.020'', 0.016'', 0.012'' and 0.010'') are investigated. Tests are performed both with and without a compression ramp installed. This direct comparison allows characterization of the effect of the SWBLI on the system dynamics. High-speed stereoscopic digital image correlation (DIC) and fast-response pressure sensitive paint (PSP) are used to obtain simultaneous full field deformation and surface pressure of the panels. The results show that the shock induced by the 20°compression ramp leads to separation of the turbulent boundary layer close to the ramp starting at about 80% of the panel length. This results in a region of large pressure fluctuations which primarily increase the vibration amplitude of the second panel mode. Analysis of the fundamental mode, which contains most of the vibration energy of the panel, shows that the SWBLI does not lead to changes of this mode, neither in frequency, amplitude or mode shape. On the other hand, analysis of the shock foot motion shows that the shock primarily oscillates at the fundamental frequency of the panel. This means that while the shock and panel oscillate at the same frequency, it is not two-way coupling. The panel vibration dictates the motion of the shock, but the shock (or rather the SWBLI) does not modify the fundamental panel vibration beyond the forcing provided by the turbulent boundary layer. Full field surface pressure predictions are made using linearized potential flow theory, which relates the local slope of the panel to the surface pressure. Results are found to be in good agreement in the region of attached flow.

I. Nomenclature

M	=	Mach number
p_c	=	cavity pressure
p	=	surface pressure
Δp	=	pressure difference ($p_c - p$)
f_s	=	sampling frequency
h	=	panel thickness
x	=	stream-wise coordinate
y	=	span-wise coordinate
w	=	out-of-plane panel deformation
x_{SSF}	=	surrogate shock foot stream-wise position

*Graduate Student, member
†Graduate Student, member
‡Lecturer, member
§Research associate, member
¶Professor, associate fellow
‖Professor, fellow

II. Introduction

High-speed vehicles operating in supersonic flow regimes are subjected to a variety of loads arising from effects such as aero-thermal heating, compressible flow phenomena and turbulence-induced broadband excitation. The interaction of high-speed flows and structural dynamics is complex, and requires significant effort in numerical modeling as well as experimental measurements [1–3]. The interaction becomes even more complex when shock waves interact with the boundary layer and lead to flow separation. Such interactions are subject to several experimental and numerical studies [4–11] that aim to better understand the underlying physical relations with the goal of creating improved numerical modeling techniques. It is established that shock wave boundary layer interactions (SWBLIs) involving supersonic flow over a compression ramp exhibit unsteady behavior [12]. This unsteadiness can be exacerbated by structural compliance, such as when the SWBLI occurs over a thin panel, and can lead to large amplitude structural vibrations [13].

An important fluid-structure interaction (FSI) problem consists of the impingement of a compression shock on a turbulent boundary layer over a compliant panel. One way of creating such a flow structure (not used in this work) is by creating a shock in the upstream region on the wall opposite of the panel, which then impinges on it. Two questions are of primary interest regarding the dynamics of such a system. How does the vibration of the panel change in the presence of SWBLI? And does the structural compliance have effects on the flow, such as the shock unsteadiness? This system in particular was studied by Spotswood et al. [9, 14] in a multi year experimental campaign. Results showed especially the benefit of utilizing full field diagnostic techniques such as digital image correlation (DIC) and pressure sensitive paint (PSP), as well as the importance that heating of the flow can have on the panel response. A similar SWBLI occurs just upstream of a compression ramp, which leads to a shock system with a detached compression shock that impinges on the boundary layer and can separate the flow. This problem for example was investigated by Schöneich et al. [11], who analyzed the effect of compliance of the ramp on the system behavior.

In the present study a set of thin brass panels of length 4.8" and width 2.5" and different thicknesses (h=0.020", 0.016", 0.012" and 0.010") are inserted into a rectangular cutout in the floor of a Mach 2 wind tunnel. A 20° compression ramp is located immediately downstream of the panel insert. This system creates a SWBLI on the compliant panel. To evaluate the effect of the SWBLI on the panel dynamics, each panel is tested twice, once without the ramp and then with ramp. This allows isolation of the system changes that result from the presence of the SWBLI. All flow parameters remain unchanged in-between the two consecutive test runs. Using high-speed DIC, the out-of-plane panel deformation is measured. A system identification technique known as complexity pursuit (CP) is utilized to obtain the mode shapes of the panel. The flow-facing side of the panel is painted with pressure sensitive paint and recorded at 50 kHz, resulting in the full field surface pressure. Deformation and pressure are measured synchronously, which allows computation of correlation between the two. Linearized potential flow theory is then used to predict surface pressure fields from the deformation of the panel.

The present study uses lessons learned from previous work performed in the field, especially with respect to measurement techniques and fabrication of test articles. On the other hand, this study adds novelty to the field by utilizing new algorithms (e.g. Complexity Pursuit for system identification), its parametric approach (multiple panel thicknesses) and its direct comparison between test cases without and with ramp. In section III the setup of the experiments is described along with details regarding the measurement techniques. Section IV contains the results of experiments performed to characterize the dynamic behavior of the panels in different conditions (no flow, flow without ramp, flow with ramp). The last section summarizes all insights gained from this study and discusses remaining open questions.

III. Experimental setup and measurement techniques

This section discusses the wind tunnel test facility as well as the experimental setup and measurement techniques used. The design and fabrication process of the test articles is also elaborated.

A. Mach 2 wind tunnel

All experiments were performed in the Mach 2 blow-down wind-tunnel of The University of Texas at Austin. The approximate flow conditions in the test section are known from previous studies [15, 16] that utilized particle image velocimetry and are listed in table 1. In the present study the free stream pressure and stagnation chamber pressure were measured. From these values the unit Reynolds number Re_∞ and stagnation pressure were computed. The computed Reynolds number was only 3% higher than that of the referenced study and thus it is assumed that the previously measured turbulent boundary layer height δ_{99} =12.5 mm (based on free stream velocity of $0.99U_\infty$) remained valid for this study.

Study	Velocity U_∞ [m/s]	Stagnation pressure p_0 [kPa]	Stagnation Temperature T_0 [K]	Boundary Layer thickness δ_{99} [mm]	Re_∞ $[m^{-1}]$
Ref. [15]	510	261 ± 7	292 ± 5	12.5	98×10^6
Present		378	285 ± 3		102×10^6

Table 1 Wind tunnel flow parameters from previous study and present study

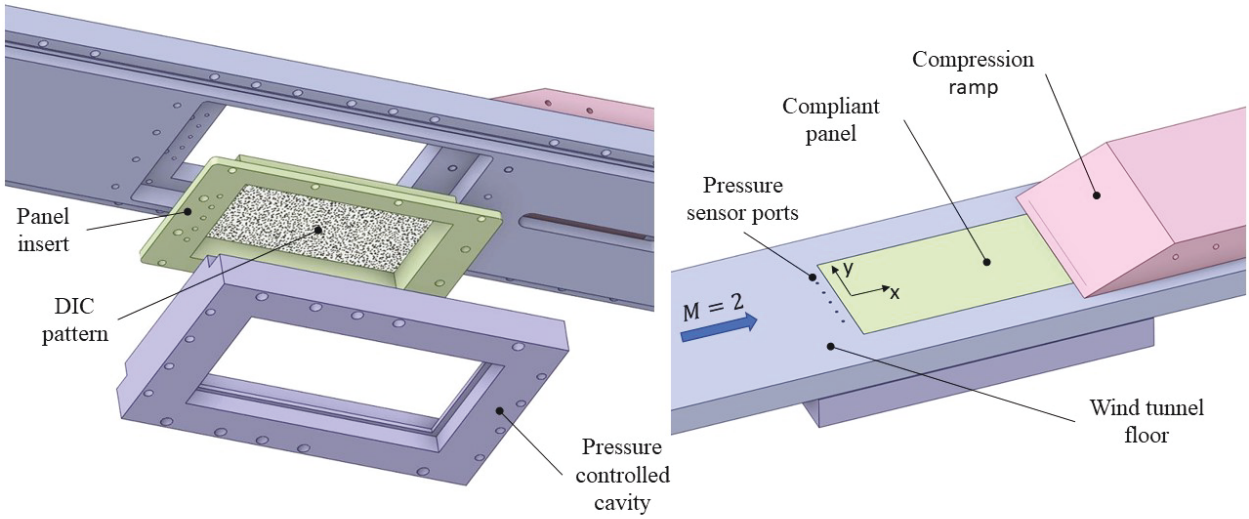

Fig. 1 Panel insert in wind tunnel floor.

B. Experimental setup

The floor of the wind tunnel test section had a rectangular cutout of width and length 2.9" × 5.2". The compliant panel insert was bolted in the cutout of the wind tunnel floor. Figure 1 shows the tunnel floor with the panel insert. A rectangular enclosure with a window on the bottom side and open on the top was attached to the lower side of the tunnel, enclosing the compliant panel. A pressure transducer (Baratron 626A, range 0-19.3 psia) and a vacuum pump were attached to this cavity through an opening at the side. There were five small holes in the wind tunnel floor section just upstream of the panel along the spanwise direction. These connected the tunnel test section to the cavity and could be used to insert Kulite pressure transducers. In most test cases, the center hole was filled with a pressure transducer and the remaining ones were plugged, so that no airflow occurred between cavity and test section. A 20° compression ramp was positioned just downstream of the panel insert. The width of the ramp was slightly more than the width of the panel insert, but less than the test section. Fences of height 0.5" were fixed to the sides of the ramp in the streamwise direction (not shown in Fig. 1) to reduce cross-stream flow over the sides of the ramp.

The full experimental setup is depicted in Fig. 2. Two cameras were setup below the tunnel at a slight relative angle viewing the lower side of the panel. They were spaced approximately 18" apart from each other at a distance of 32" below the panel. This stereoscopic setup was used to measure the panel deformation with 3D-DIC. An LED array placed in-between the cameras illuminated the speckle pattern to ensure sufficient contrast in the images. Details regarding the DIC setup are provided in section III.C. Just above the tunnel test section, a third camera was installed which viewed the flow-facing-side of the panel through a window installed in the tunnel ceiling. This camera was used to measure the surface pressure on the panel with PSP. An additional LED located above the tunnel served to illuminate

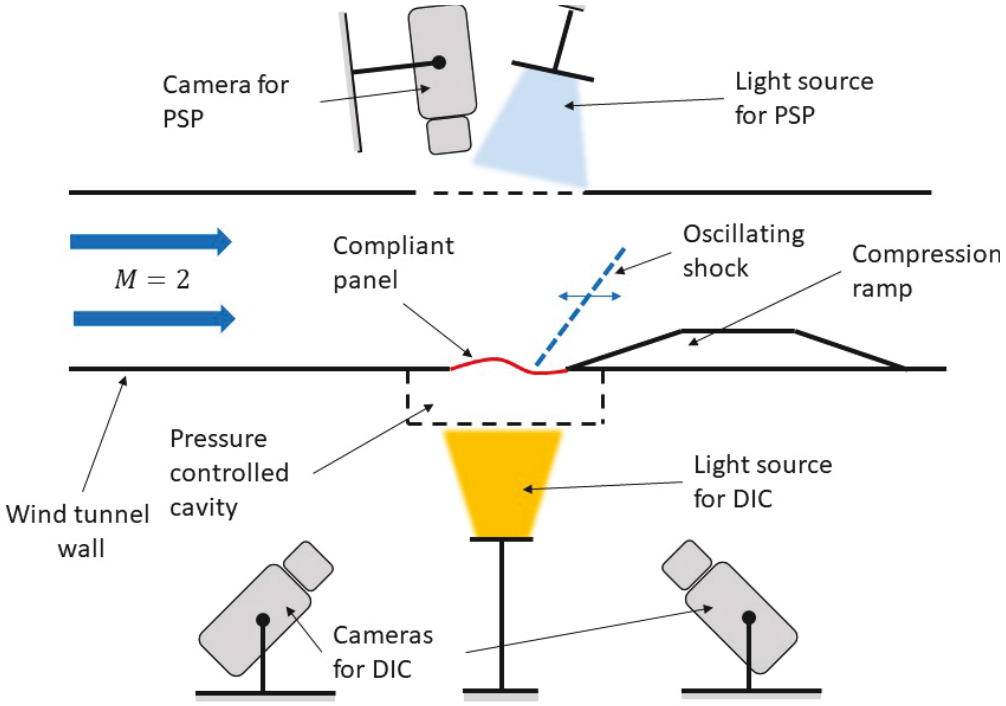

Fig. 2 Full experimental setup at wind tunnel.

the PSP. Details regarding the PSP setup are provided in section III.D.

During a wind tunnel run, four systems were running simultaneously. The PSP system measured the surface pressure, the DIC system measured the panel deformation, a Kulite pressure transducer measured the free stream pressure p_∞ upstream of the panel and an additional transducer measured the pressure p_c within the cavity. Two separate computers were used in this setup. PC-1 ran the software (Davis 10.1 by LaVision) that controlled the cameras used for DIC. PC-2 ran the software (Photron PFV4) to control the camera above the tunnel, hereafter referred to as the PSP camera. To initiate a measurement, a TTL trigger signal was generated by the PFV4 program on a user command and sent from the computer (PC-2) to the PSP camera, which then started recording. The trigger signal was sent to a timing unit (LaVision portable timing unit (PTU)), which controlled the cameras located below the tunnel (hereafter referred to as the DIC cameras). Similar to the trigger signal, the 50 kHz clock signal on which the PSP camera ran (it recorded at f_s =50000 frames per second), was forwarded to the PTU. The DIC cameras recorded only at f_s=5 kHz and thus the original clock signal was first down-sampled. This was done using two timing boxes (Stanford Research Systems, DG535), which converted the high frequency signal to a synchronized low frequency signal. The trigger signal which started the recording of all three cameras was also sent to a data acquisition system (cDAQ by National Instruments). The cavity pressure sensor was attached to this cDAQ. Similarly, the Kulite pressure transducer was sampled at 100 kHz and connected to a separate data acquisition system (PXIe by National Instruments).

A set of four compliant panels was fabricated, varying in thickness (h = 0.010", h = 0.012", h = 0.016", h = 0.020"). Each panel was made from 260 brass shim stock of length and width 4.8" and 2.5" respectively. Each shim was bonded to a brass base, to form a single panel insert, that could be bolted into the tunnel test section. The base contained a 0.2" wide ledge on which solder paste was applied, see Fig. 3a. The shim was then pressed onto the base and heated in a small oven until the solder melted and bonded the panel to the insert, see Fig. 3b. The bondline proved strong enough to withstand static shear and vibratory loads during all wind tunnel runs and no failure was observed.

C. High-speed digital image correlation (DIC)

Two monochromatic high-speed cameras (Phantom Miro M310) were used to measure structural deformation of the panel. Each camera was equipped with a Scheimpflug adapter as well as a 105 mm Nikon lens with an F-stop setting of 5.6. The cameras were controlled using the software DAVIS 10.1 by LaVision, which performed synchronization of

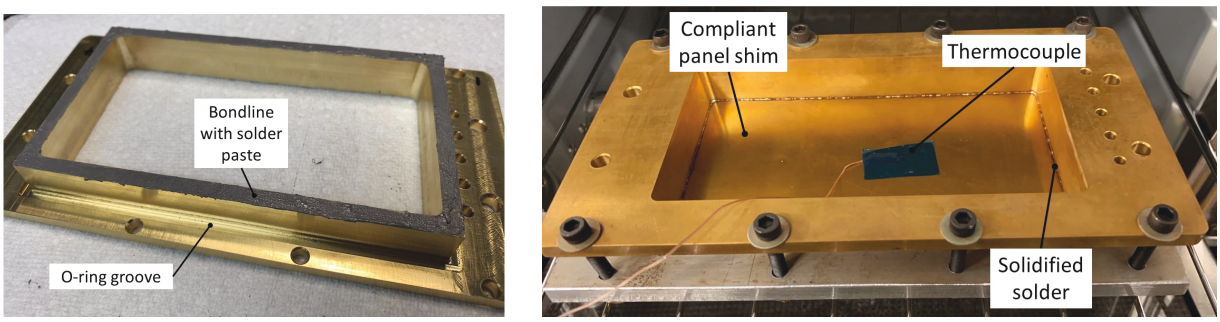

(a) **(b)**

Fig. 3 Reflow soldering process of panel, (a) solder paste on base, (b) sandwiched panel insert in oven with thermocouple.

the cameras, calibration as well as the DIC computation in post-processing. A speckle pattern was created by using the open source Python code "speckle_pattern.py" from the Laboratory for Dynamics of Machines and Structures at the University of Ljubljana, Croatia. The speckle pattern was custom made for the specific camera setup to result in randomly distributed blurry speckles with diameters not exceeding seven pixels. The pattern was printed onto a thin adhesive paper (AVERY address label, thickness 0.0054") and carefully attached to the DIC side of the panel. The stereoscopic DIC system was calibrated using the DAVIS calibration routine. A calibration pattern was printed and glued onto a flat surface and images were taken at nine different out-of-plane locations, spaced 0.5 mm apart. A third order polynomial mapping function was then curve-fit to map the camera coordinate system to the real world coordinates. The reported root-mean-square error of the fit was 0.17 px (28 μm). A set of 100 images was recorded of the motionless panel, to determine a noise floor. The temporal standard deviation of the noise floor for the out-of-plane deformation was approximately 3 μm for most of the panel area. The sampling frequency was set to f_s = 5000 Hz with an exposure time of 100 μs. Data was recorded for a duration of 2 seconds once steady flow conditions were observed. An LED array was used in continuous mode to illuminate the speckle pattern.

D. High-speed pressure sensitive paint (PSP)

Polymer/ceramic pressure sensitive paint was used to obtain fast response, full field surface pressure data. The paint is based on the luminophore ruthenium whose emission of light is quenched by oxygen, thus allowing its use for pressure sensing applications. The polymer/ceramic PSP was mixed on location and sprayed directly onto the flow-facing side of the panel using a spray gun (Paasche Airbrush H0318). The binder consisted of a mixture of silicone and TiO_2 particles. The mixing and painting was done on the day prior to each experiment. During the wind-tunnel run, a custom built blue LED light (peak wavelength at 460 nm) excited the paint. Its design was based on the CBT-120 LED chip by Luminus. The light was operated in continuous mode for the entire duration ($\approx$ 2 s) of the image acquisition time. Images of the PSP were recorded using a Photron Mini Fastcam AX50. A 35 mm focal length Nikon lens was used with an f-stop value of 2. The frame rate was set to f_s=50 kHz with an exposure time of 10 μs. The frame rate was set higher than the maximum frequency response of the PSP (around 20 kHz) to reduce aliasing effects.

IV. Results and discussion

A. Structural tests without flow

1. Effect of DIC sticker and PSP on modal parameters

A set of tests was performed to quantify the effect of adding a thin layer of paint (PSP) as well as the adhesive speckle pattern sticker on the structural dynamics of the panels. A one inch wide rectangular beam was cut from shim of the same material as the panels (260 brass, h = 0.031") and the DIC sticker and paint were attached. The beam was then clamped at one end to create a cantilever beam with a free length of 6". An impact hammer (PCB, modally tuned, with load cell) was used to hit the beam near its root and a capacitive displacement sensor (Micro-epsilon

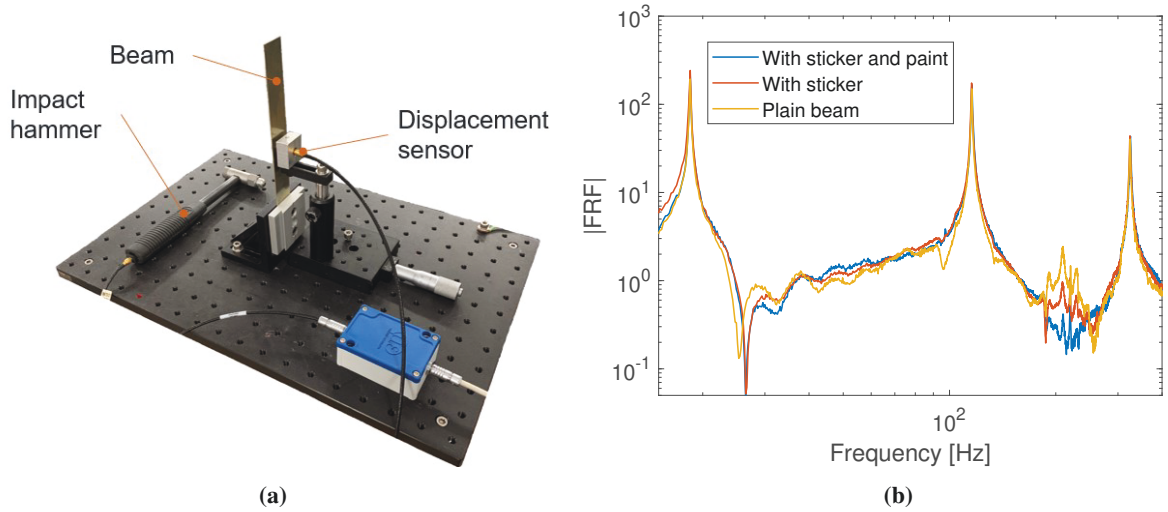

Fig. 4 Cantilever beam impact; (a) test setup and (b) FRF.

capaNCDT 6110 CS05) was utilized to record the vibratory response approximately one inch from the clamped end. The setup is shown in Fig. 4a. From the measured input force and response, the frequency response function (FRF) was calculated and is shown in Fig. 4b. The plot clearly shows three peaks corresponding to the first three modes of the cantilever beam. In a next step, the paint was removed from the beam and the impact test was repeated. Then, the DIC sticker was removed using acetone and the test was repeated once more. The beam was not removed from its clamped support during the removal of paint and DIC sticker to avoid accidentally changing the boundary conditions. Using the signal processing toolbox of MATLAB, a 3-dof system was curve fit to each FRF respectively using the 'peak picking' technique, which resulted in the natural frequencies f_i and damping ratios ζ_i. The results show that the addition of the paint and DIC sticker had no effect on the natural frequencies within experimental error. A noticeable difference was measured regarding the damping, where a relative increase of up to 20% was seen in the first mode. The test was repeated for a beam cut from the thinnest shim (h=0.010"). Similar results were obtained and no significant change in natural frequency was measured as a result of the DIC sticker and paint.

2. Effect of in-plane stresses on modal parameters

The natural frequencies of each panel are a function of its material parameters (density ρ, Young's modulus E), its dimensions (length L, width W and thickness h) and its boundary conditions. By performing an experimental modal analysis (impact testing), the natural frequencies can be determined. A strictly linear structural plate model (based on Kirchhoff theory) exhibits natural frequencies that are independent of external loading. A non-linear model also considers in-plane stresses, which can modify the bending stiffness of a plate and thus change its natural frequencies. The in-plane tensile stresses can result for example from large out-of-plane deformations or thermal gradients (mismatch between temperature of panel and panel support).

In order to characterize this non-linear effect, a set of impact tests was performed while a static pressure difference was applied to the panel. The pressure difference resulted in out-of-plane deformation, which in turn led to in-plane tensile stresses. Using both a vacuum pump and a compressor, the pressure was modified in the cavity resulting in a bulging of the panel into and out of the test section. The panel was directly impacted near its corner using an impact hammer and the response was measured with a capacitive displacement sensor located near (but not exactly at) the center. An average of three impacts was taken to compute the FRF at each pressure value and the fundamental frequency was calculated. The resulting plots for the four panels are shown in Fig. 5.

For an ideally fabricated panel with no pre-stress, the lowest natural frequency should occur at the pressure equilibrium state at ΔP=0 psi and the frequency increase should be symmetric for changes in pressure around that point. This trend was generally well observed with all four panels.

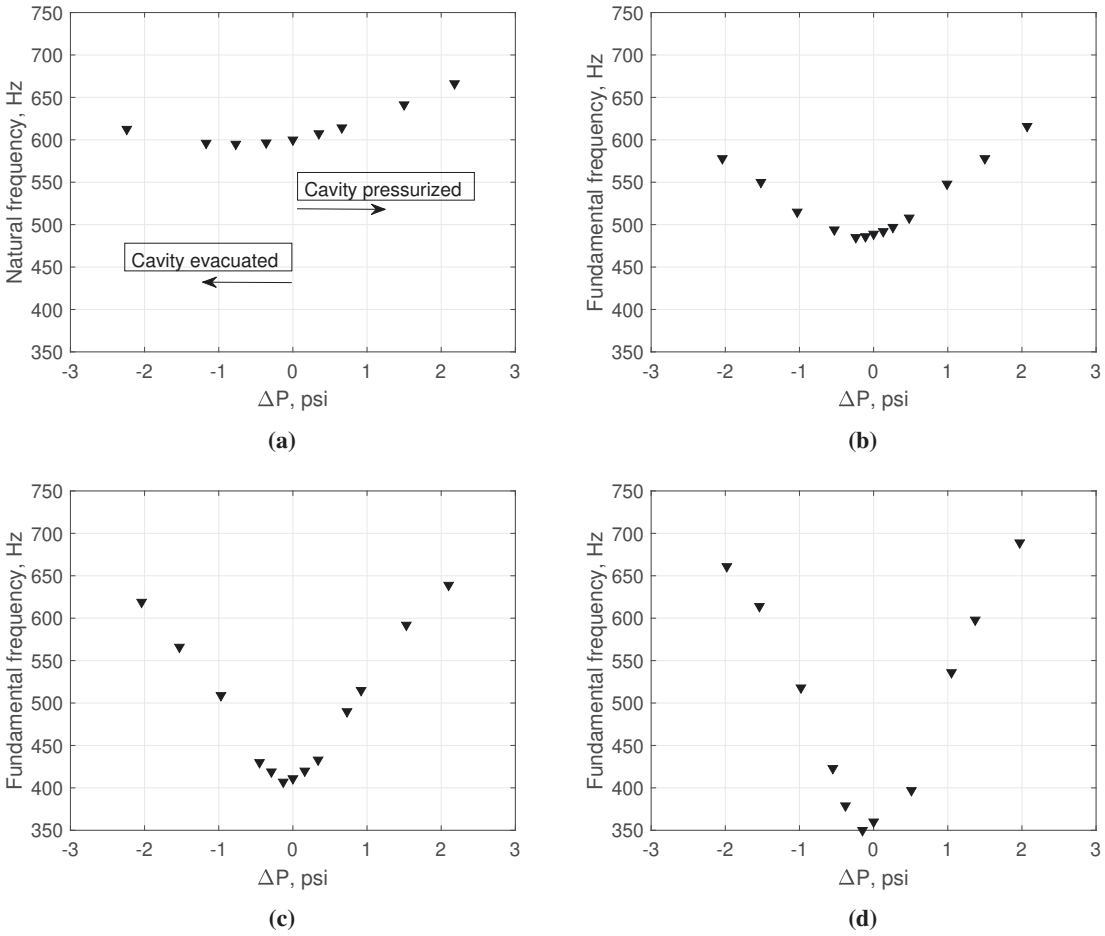

Fig. 5 Effect of static pressure difference on fundamental frequency, (a) $h = 0.020$”**, (b)** $h = 0.016$”**, (c)** $h = 0.012$”**, (d)** $h = 0.010$”**.**

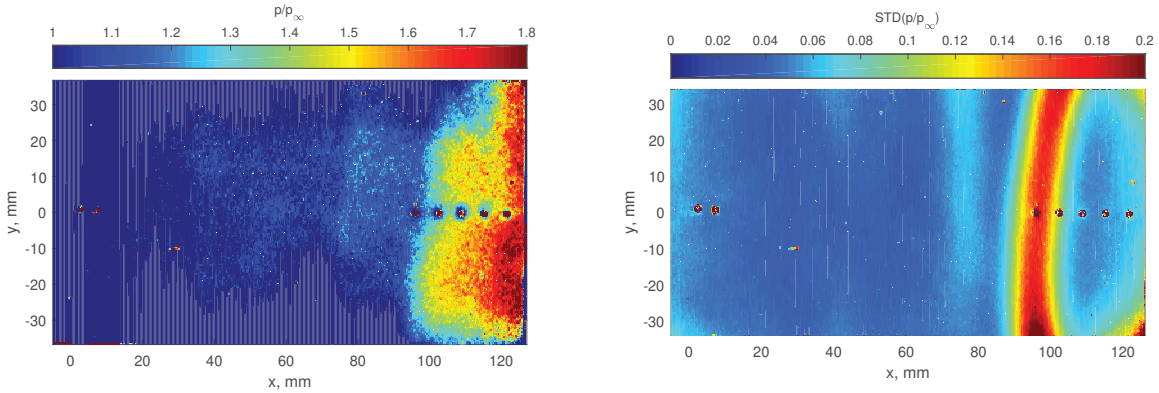

(a) **(b)**

Fig. 6 Surface pressure measurements from PSP on rigid panel with ramp; (a) instantaneous pressure field and (b) standard deviation; flow from left to right.

B. Effect of ramp on panel response

1. Nature of the pressure forcing

Before the structural response of the panels is analyzed, a look at the forcing function, e.g. the pressure field is in order. A test with the compression ramp was performed on a rigid panel insert to obtain information about the surface pressure field without compliance of the panel. The spatial distribution of the standard deviation of the surface pressure was computed for this test. At each location on the panel the time-history of the normalized pressure p/p_∞ was extracted and its standard deviation was computed. A surface plot of the resulting standard deviation values was then created and shown in Fig. 6b. The plot shows clearly the intermittent region of the separation shock foot, which leads to a thin band of large pressure fluctuations, approximately 10 mm wide. An example of an instantaneous surface pressure field is shown in Fig. 6a, which clearly shows the region of increased pressure downstream of the shock foot around x = 100 mm. The rigid panel insert featured seven small holes along the centerline, that were used to calibrate the PSP.

2. Analysis of deformation power spectra

Shown in Fig. 7 are deformation power spectra of a single point on each of the four panels. The point location is at x=90 mm, y=-10 mm and was chosen to avoid nodal points of the lower panel modes. This point is labeled as reference point "B" in fig. 7a. The power spectra are computed using Welch's method, which reduces the noise in power spectral density by averaging windowed subsets of a time-history. The total number of 10000 data points (two seconds recorded at f_s=5 kHz) is divided into subsets of length 1000 with an overlap of 500 data points and multiplied with a Hamming window. The frequency content below 200 Hz is not plotted since that region is well below the fundamental frequency for all panels. Each plot shows the comparison between two successive runs, one without the ramp and one with the ramp installed. Since no parameters apart from the ramp were changed in-between these two runs, the difference in response should be only due to the effects of the ramp-induced SWBLI. Several effects are noticeable from these plots:

The response of each panel contains multiple structural modes as can be seen by the distinct peaks in the power spectra. The response is dominated by the fundamental mode, which is the largest peak in each spectrum. The amplitude of the response grows as the panels become thinner. Surprisingly, for all panels the SWBLI hardly affects the fundamental mode. Both amplitude and frequency remain mostly constant. The second mode (second lowest frequency peak) is most affected by the SWBLI. The inclusion of the ramp significantly increases the amplitude of vibration of the second mode. This can be explained by looking at Fig. 6b, where the standard deviation of the pressure field is shown on a rigid panel for a test case with ramp. The region of shock intermittence is characterized by large pressure fluctuations (large forcing on the structure). The second panel mode consists of a nodal line near x = 66 mm with two asymmetric peaks, one downstream and and one upstream. The large pressure fluctuation region is located near the downstream peak of the second mode and thus primarily excites that mode through geometric forcing. Note that the

plots generally show also an increase in vibration of higher modes due to the SWBLI, though it is not as prominent.

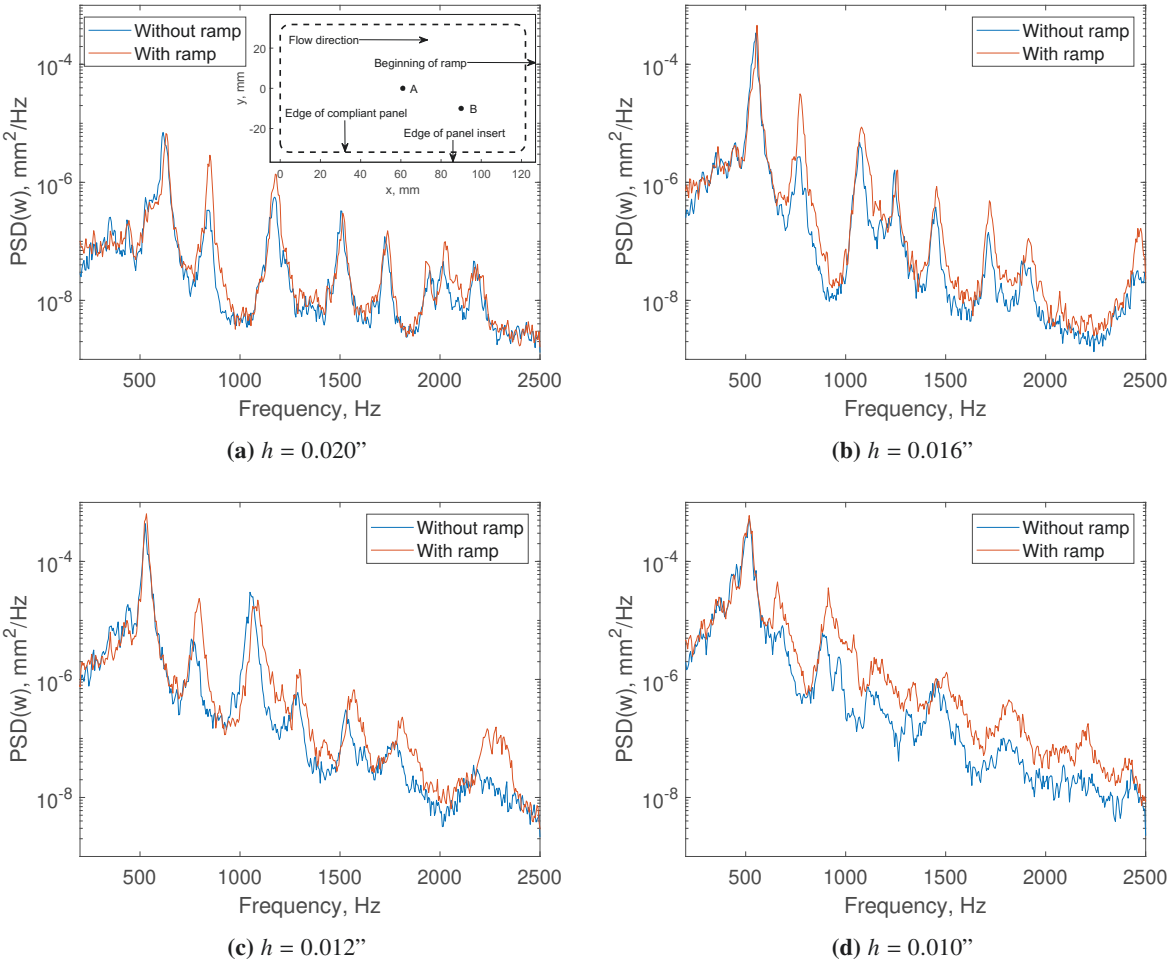

(a) h = 0.020” **(b)** h = 0.016”

(c) h = 0.012” **(d)** h = 0.010”

Fig. 7 Deformation power spectra at reference point "B" from DIC, (a) h = 0.020”**, (b)**h = 0.016”**, (c)** h = 0.012”**, (d)** h = 0.010”**.**

3. Operational modal analysis

The power spectra of the previous section show that the ramp-induced SWBLI increases panel vibration of the second structural mode. Most of the vibrational energy in the system however is contained in the fundamental mode. The local power spectra indicate that SWBLI has virtually no effect on the fundamental mode vibration, neither in frequency nor amplitude. This is made clear by analyzing the behavior of the fundamental mode shape. Using a system identification algorithm known as complexity pursuit (CP) developed by Stone [17], the dynamic response of the panel measured with DIC can be decomposed into its modes. Shown in Fig. 8 is the fundamental mode shape for each of the four panels. The mode shapes in the left column represent test cases without the compression ramp and the column on the right shows test cases with the compression ramp. Several conclusions can be drawn from the figure as follows:

By looking only at the left column (test cases without the ramp) the fundamental mode for each panel seems to be skewed in the downstream direction. This is evidence of fluid-structure coupling (panel motion couples with attached flow) and the direction of the skew is based on the flow direction. Even very simple aeroelastic theory is able to predict this effect at least qualitatively, see e.g. Refs. [18, 19]. The coupling between flow and structure becomes stronger for higher dynamic pressures and thinner panels. Since the flow conditions (and thus the dynamic pressure) are kept constant, only the compliance of the panels changes. The thinner panels couple stronger with the flow than the thicker ones, which can be seen by the increasing downstream skew of the mode shapes as the panels become thinner in Fig. 8.

A second conclusion that follows from these results is that the SWBLI has essentially no effect on the fundamental mode shape. This can be seen by comparing the mode shapes of the left and right column. Qualitatively, they seem the same. A qualitative comparison between two mode shapes (without and with flow) is made by computing the modal assurance criterion (MAC). The MAC represents the cosine of the angle between the two mode shape vectors. A MAC value of zero means that the mode shapes are orthogonal to each other and a value of unity means that they are identical (or rather parallel). MAC values are shown for each of the four pairs of mode shapes in Fig. 8 and they are all very close to unity (all greater than 0.995). This is a remarkable results and not intuitive. It means that even though the flow field changes drastically due to the SWBLI, there is no coupling mechanism in place which results in changes to the dominant dynamic behavior of the panel, meaning its fundamental mode vibration.

C. Correlation between pressure and deformation

The previous section only discussed the structural response of the panel, meaning the data measured with DIC. This section now takes into account the pressure field that was measured with PSP. Based on linearized potential flow theory for a flat plate [19], the surface pressure change is calculated as:

$$\Delta p(x,t) = \frac{2q_\infty}{\sqrt{M_\infty^2 - 1}} \left[\frac{\partial w}{\partial x} + \frac{1}{U_\infty} \frac{(M_\infty^2 - 2)}{(M_\infty^2 - 1)} \frac{\partial w}{\partial t} \right], \tag{1}$$

where U_∞, M_∞ and q_∞ denote the freestream velocity, Mach number and dynamic pressure. This equation is a decent approximation for flows above $M_\infty = \sqrt{2}$. A surface pressure change is thus linked to two quantities:

1) The local out-of-plane deformation gradient in stream-wise direction $\partial w/\partial x$, which is equivalent to the local wall angle.
2) The local out-of-plane deformation velocity $\partial w/\partial t$.

The first effect, which influences the stiffness of the aeroelastic system is dominant compared to the second one, which influences the system damping. The theory, which is valid for linearized inviscid supersonic flow is invalid in the presence of SWBLI, which exhibits regions of subsonic flow. The theory also only considers the local state of the panel and does not take into account its deformation history or the deformation of the rest of the panel. Upstream of the shock foot, the fundamental relation between pressure and deformation gradient should however still apply.

In the following discussion the relation between local deformation gradient and surface pressure is investigated. A full-field analysis is performed, where the time-histories of the pressure and deformation are first band-pass filtered and then conditionally averaged. The goal of this analysis is to demonstrate the validity of the linearized theory for the test cases with and without ramp and to showcase the strength of using time synchronous PSP and DIC for full-field analysis.

The full field analysis is based on conditional averaging and contains multiple steps. A flowchart of the processing steps is shown in Fig. 9. These steps are:

1) The natural frequency of a structural mode is identified by analyzing the power spectrum of the deformation at a single point on the panel.
2) A high-order temporal band-pass filter centered at the natural frequency (7th order Butterworth filter, bandwidth 40 Hz) is applied to the deformation time histories (from DIC) and the surface pressure time-histories (from PSP) of each point on the panel.
3) The deformation time history (after filtering) of a single point on the panel (e.g. at the center) is plotted. The 100 largest peaks are identified, using the 'peaks' function in MATLAB. The 100 time steps that correspond to those peaks are stored.
4) Surface plots are created of the (previously band-pass filtered) deformation at each of the 100 time steps that were just identified. These surface plots are averaged to obtain one single surface plot, which shows the deformation amplitude of the band-pass filtered data.
5) Surface plots are created of the (previously band-pass filtered) surface pressure at the same 100 time steps at which the deformation showed a peak. These surface plots are averaged to obtain one single surface plot, which shows the surface pressure amplitude of the band-pass filtered data.

The analysis is performed for the thinnest panel ($h = 0.010$") for the first two modes. For the first mode, the temporal band-pass filter is centered around 518 Hz. The resulting plots are shown in Fig. 10 for the case without and with ramp.

A focus is first placed on the case without ramp, shown in the left column. The top plot shows the deformation, which resembles closely the fundamental mode shape. From linearized potential flow theory, the first order relation

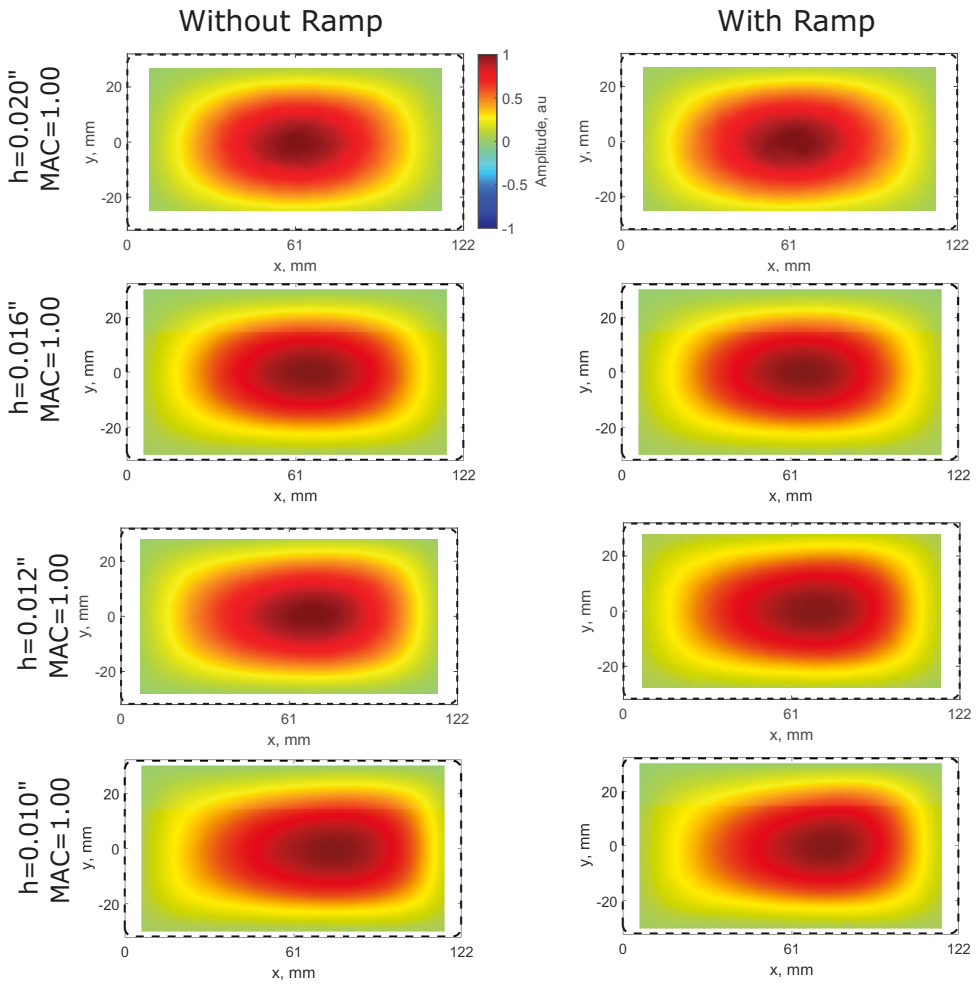

Fig. 8 Comparison of fundamental mode for test cases without ramp (left column) and with ramp (right column) for varying panel thicknesses; flow from left to right; ramp located at x=127 mm.

Step 1: Determine natural frequency from peak of single power spectrum

Step 2: Apply bandpass filter (around identified frequency) to deformation (DIC) and pressure (PSP) for all points on panel.

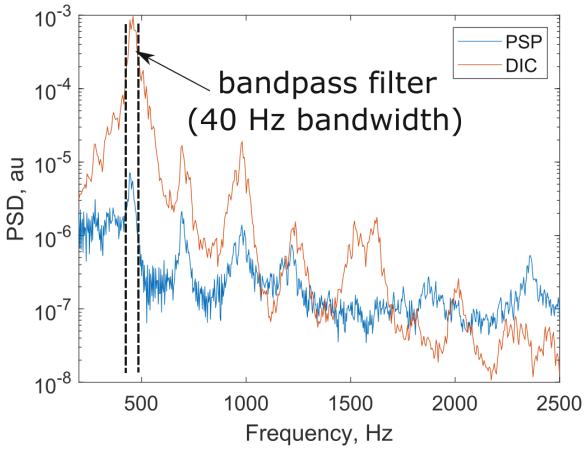

Step 3: Plot single time history of deformation (e.g. at panel center) and determine 100 largest peaks and their time steps.

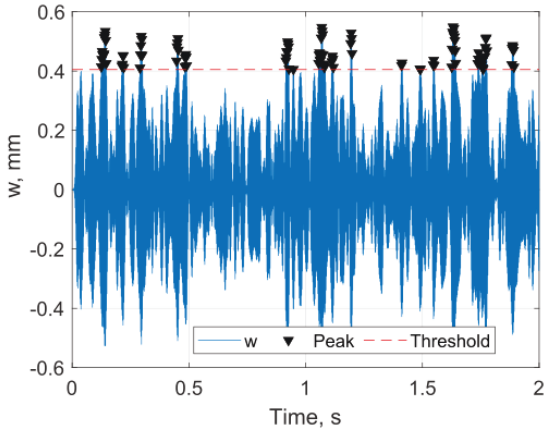

Step 4: Create plots of full field deformation at those time steps and average them.

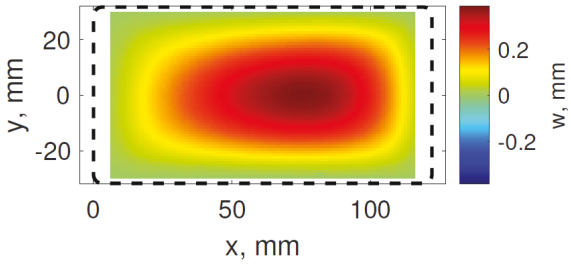

Step 5: Create plots of full field pressure at the same time steps and average them.

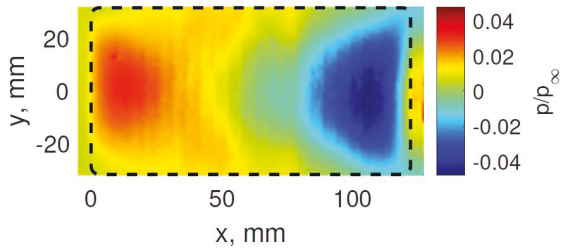

Fig. 9 Processing steps to obtain averaged pressure and deformation fields.

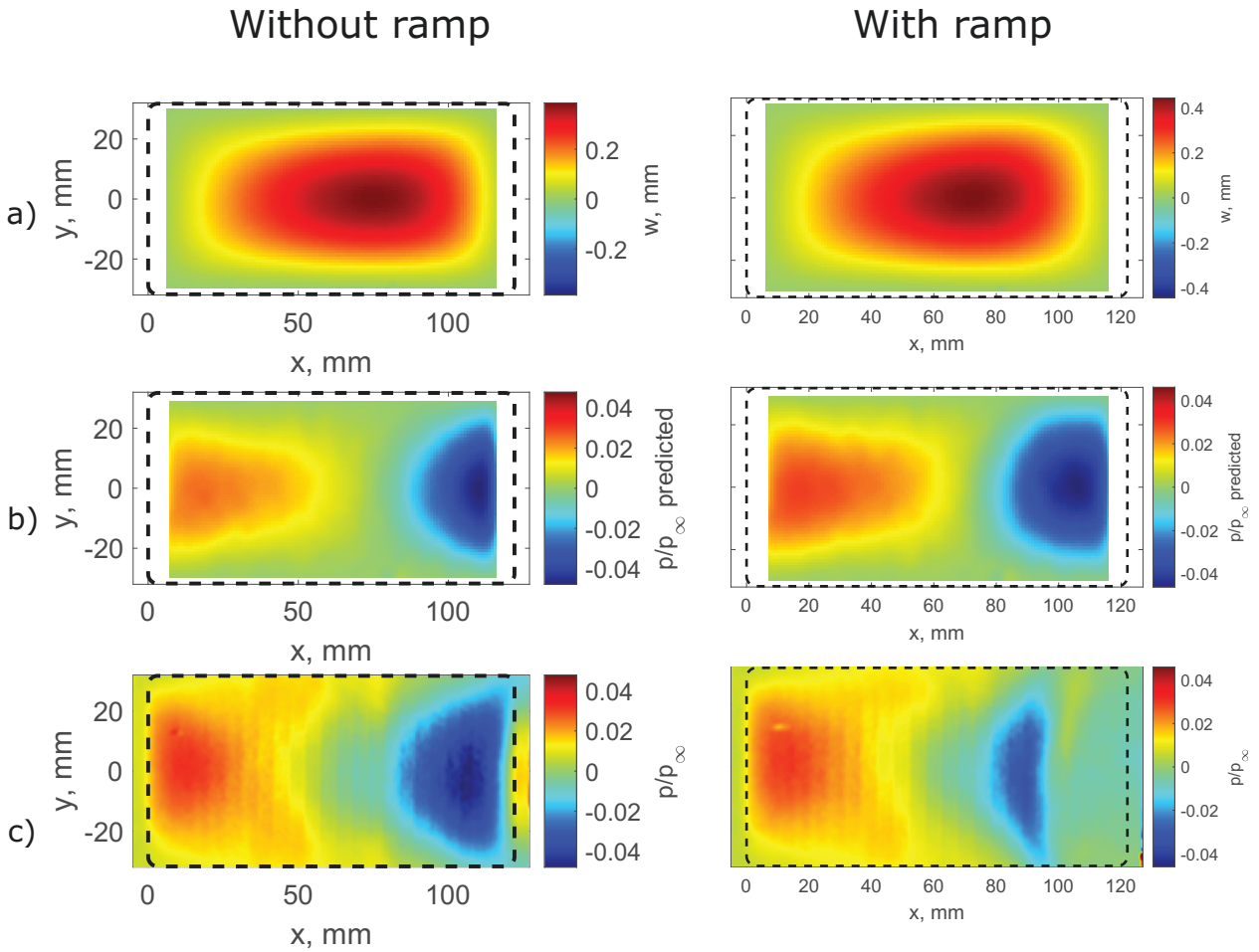

Fig. 10 Full field comparison of band-pass filtered deformation and pressure field (h=0.010", mode 1-1). (a) deformation from DIC, (b) predicted pressure field from linearized theory and wall angle, (c) measured pressure from PSP; flow from left to right.

between pressure fluctuations and deformation gradient (wall slope) is

$$\frac{\Delta p}{p_\infty} = \frac{2q_\infty}{p_\infty\sqrt{M_\infty^2-1}}\left(\frac{\partial w}{\partial x}\right) = \frac{\gamma M_\infty^2}{\sqrt{M_\infty^2-1}}\left(\frac{\partial w}{\partial x}\right) \approx 3.2\left(\frac{\partial w}{\partial x}\right)$$

The value of 3.2 is an approximation of the flow conditions obtained for a Mach number of $M_\infty = 2$ and $\gamma = 1.4$. From the deformation plot the streamwise gradient (wall slope) is computed and multiplied by 3.2 to obtain the predicted pressure field. This is shown in the middle plot of Fig. 10 (row b). The bottom plot shows the measured pressure field from PSP, which is obtained by performing the same conditional averaging of band-pass filtered data as for the DIC data. There exists good agreement between prediction and theory overall. The upstream region of the measured pressure field appears more noisy than the prediction.

The same analysis is now performed for the corresponding tunnel run with the ramp and the resulting plots are found in the right column of Fig. 10. The plots for the deformation and wall slope look similar to the case without ramp. There is a clear discrepancy between the predicted and measured pressure field for $x > 100$ mm, which is the region of separated flow. As expected, the linear theory is not able to predict the pressure in that region, though the prediction works relatively well in the region upstream of the flow separation.

The same analysis is performed for the second mode. The plots are shown in Fig. 11. Once again, the predicted and measured pressure fields match nicely in the regions of attached flow, but prediction fails downstream of the shock impingement. Similar results are found for the third mode, though the plots are omitted here for conciseness.

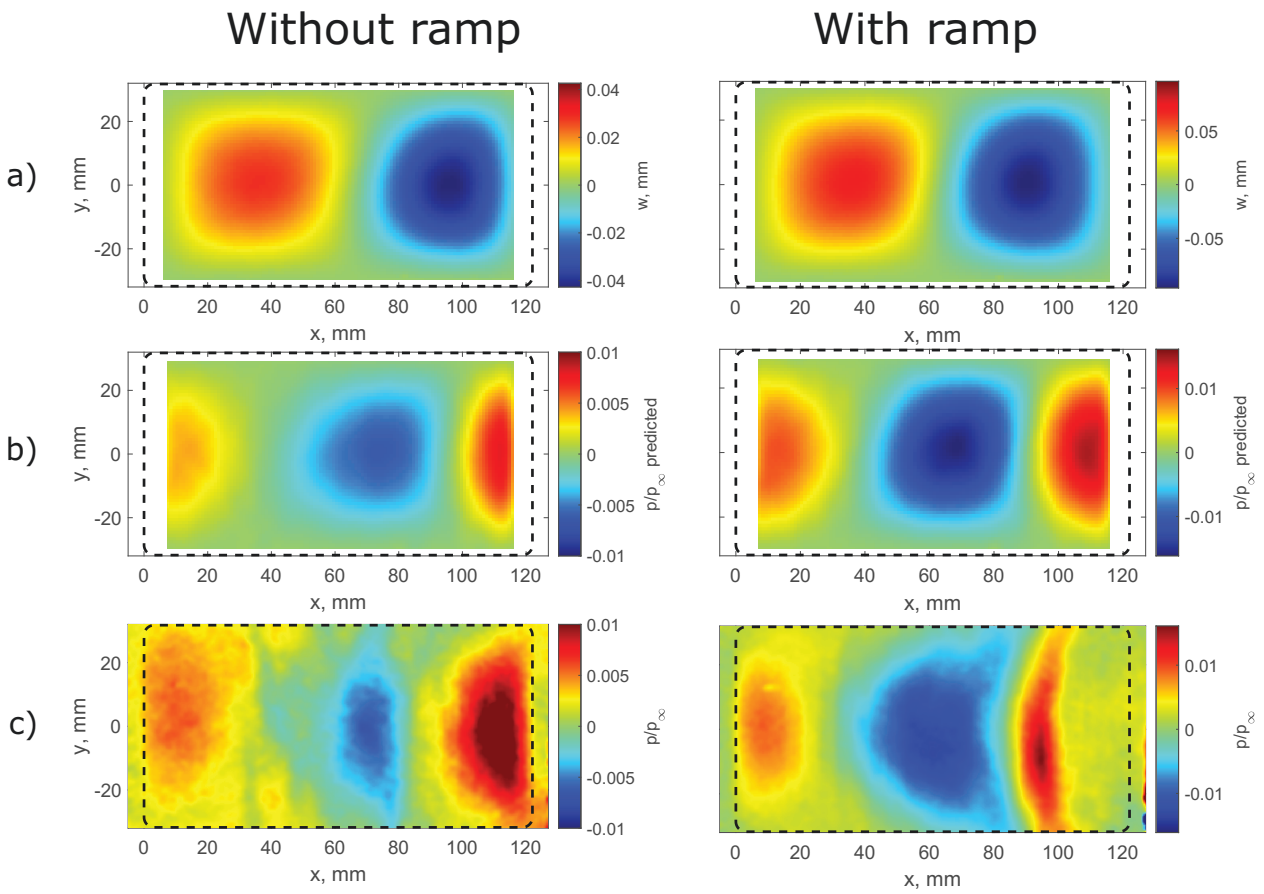

Fig. 11 Full field comparison of band-pass filtered deformation and pressure field (h=0.010", mode 2-1). (a) deformation from DIC, (b) predicted pressure field from linearized theory and wall angle, (c) measured pressure from PSP; flow from left to right.

D. Shock foot motion

The analysis so far has focused mostly on how the surface pressure field is affected by the structural vibrations. These surface pressure oscillations are local effects which might not be of importance to other parts of a flight vehicle. In contrast to that is the motion of the compression shock, which can have large influences on other structural surfaces on which it impinges. The motion of the shock foot is discussed, based on measurements from PSP.

A common method used to measure the location of the compression shock is to estimate the shock foot position from the surface pressure. For this purpose, the pressure data obtained using PSP is used. A surrogate shock foot, hereafter referred to as SSF, is defined based on a surface pressure value. Unlike in the free stream, where a shock is characterized by a discrete pressure jump, surface pressure rises much more gradually in the location where the shock interacts with the boundary layer, see e.g. Ref. [20]. In the present study, a pressure threshold value is defined separately for each test based on visual inspection of the surface pressure data from PSP. The shock position is then estimated using a MATLAB routine consisting of several steps. First, the pressure field obtained from PSP is binarized, meaning each pixel either is assigned a value of zero or one, based on the user defined pressure threshold. A set of interpolations is performed next, which fill small holes in the high and low pressure regions. The algorithm then obtains the edge between the two regions and stores the location of that line as a single vector. This process is then repeated for all time steps. The computation is based on functions available in the MATLAB image processing toolbox; a computationally cheap process, which can be performed within seconds for thousands of images on a regular desktop computer.

The power spectral densities of the shock foot motion x_{SSF} at the centerline are computed for each panel and are shown in Fig. 12. In each plot, the frequencies of the first three panel modes are shown as vertical lines. The panel modes are obtained from the DIC data using the CP algorithm. The plots show that the shock primarily oscillates at the same frequency as the fundamental mode of the panel. This shock motion becomes larger for the thinner panels, where the vibration amplitudes are also larger.

The analysis performed in previous sections shows that the SWBLI does not modify the fundamental mode of the panel, neither its mode shape nor its frequency or amplitude. This means that while the shock and panel oscillate at the same frequency, it is not two-way coupling. The panel vibration dictates the motion of the shock, but the shock (or rather the SWBLI) does not modify the dominant first mode panel vibration.

V. Summary and Conclusion

This study investigated the interaction between a Mach 2 flow over a 20° compression ramp and a compliant panel. The goals of this work were to investigate the effect of the ramp-induced SWBLI on the dynamics of the system. Panels of different thicknesses were investigated and thinner panels generally showed larger vibration amplitudes and stronger fluid-structure coupling. High-speed stereoscopic DIC and fast-response PSP were used to obtain time resolved, synchronous structural deformations and surface pressure fields. Linearized potential flow theory was used to predict pressure maps using the local wall angle of the deformed panel. Results showed good agreement, though the prediction is not valid in the region near the ramp were the flow was separated. This analysis demonstrated the advantage of time resolved, synchronous DIC and PSP for the measurement of this type of coupled system. Deformation power spectra showed that the SWBLI primarily increased the vibration amplitude of the second structural mode, without significant effect on the fundamental mode. This was further shown by comparing fundamental vibration mode shape for test cases without and with ramp; the mode shapes remained unchanged. While the SWBLI did not affect the fundamental panel mode, the fundamental panel mode affected the SWBLI. This was shown by analyzing the motion of the shock foot, which oscillates primarily at the fundamental structural mode frequency. The results presented in this paper indicated that for the given flow conditions and choice of structural parameters, the dynamics of the fluid-structure system remain mostly unaffected by the presence of ramp-induced SWBLI. Thus, satisfactory approximations of the system can be made by considering the much simpler case of a turbulent boundary layer over a flat panel first and assuming vibration of the shock foot at the fundamental frequency of the panel. Only the vibration of the second mode was increased by the SWBLI through geometric forcing, an effect which could be tackled by aeroelastic tailoring of the panel. Local stiffening of the panel may significantly increase its resilience to this localized forcing stemming from the shock intermittent region. This aspect will be investigated in future work. Results showed also some effect of SWBLI on the vibration of higher modes, such as some changes in natural frequency and vibration amplitudes. More detailed analysis of the effect of SWBLI on higher structural modes, and their mode shapes are subjects of future investigations as well.

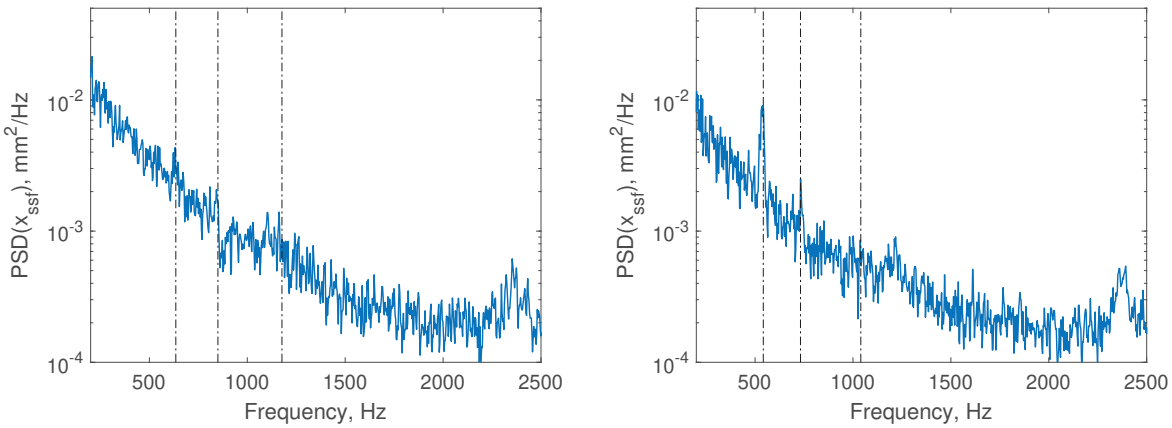

(a) h=0.020" **(b) h=0.016"**

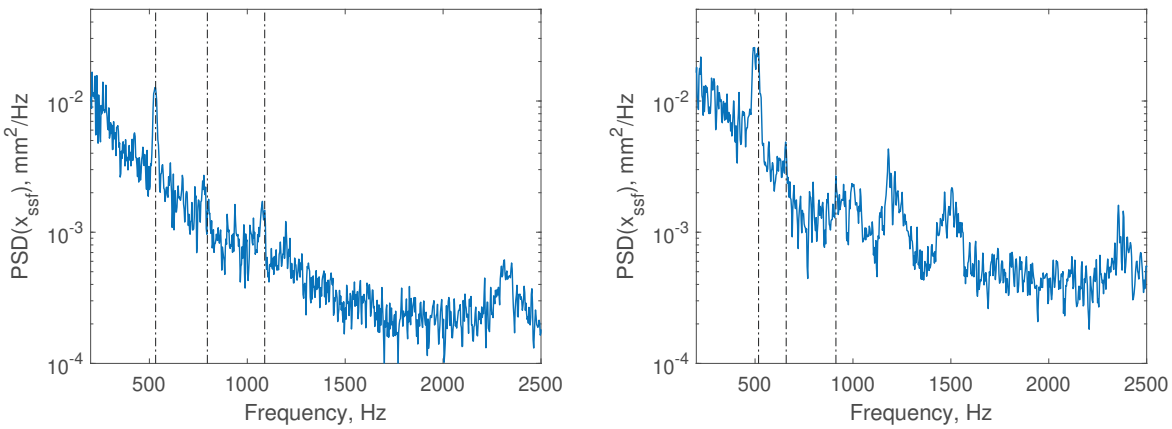

(c) h=0.012" **(d) h=0.010"**

Fig. 12 Motion of shock foot in stream-wise direction at centerline. Dotted lines denote first three structural modes.

Acknowledgments

This work was supported by the National Science Foundation under award # 1913587. The authors would like to thank Jeremy Jagodzinski for assisting with the measurements.

References

[1] Frendi, A., "Coupling Between a Supersonic Turbulent Boundary Layer and a Flexible Structure," *AIAA Journal*, Vol. 35, No. 1, 1997, pp. 58–66. https://doi.org/10.2514/2.87.

[2] Mei, C., Abdel-Motagaly, K., and Chen, R., "Review of Nonlinear Panel Flutter at Supersonic and Hypersonic Speeds," *Applied Mechanics Reviews*, Vol. 52, No. 10, 1999, pp. 321–332. https://doi.org/10.1115/1.3098919, URL https://doi.org/10.1115/1.3098919.

[3] Casper, K. M., Beresh, S. J., Henfling, J. F., Spillers, R. W., Hunter, P., and Spitzer, S., "Hypersonic Fluid–Structure Interactions Due to Intermittent Turbulent Spots on a Slender Cone," *AIAA Journal*, Vol. 57, No. 2, 2019, pp. 749–759. https://doi.org/10.2514/1.J057374.

[4] Maestrello, L., and Linden, T., "Measurements of the response of a panel excited by shock boundary-layer interaction," *Journal of Sound and Vibration*, Vol. 16, No. 3, 1971, pp. 385–391. https://doi.org/https://doi.org/10.1016/0022-460X(71)90594-3.

[5] Willems, S., Gülhan, A., and Esser, B., "Shock induced fluid-structure interaction on a flexible wall in supersonic turbulent flow," , 2013. https://doi.org/10.1051/eucass/201305285, URL https://doi.org/10.1051/eucass/201305285.

[6] Brouwer, K. R., Gogulapati, A., and McNamara, J. J., "Interplay of Surface Deformation and Shock-Induced Separation in Shock/Boundary Layer Interactions," *AIAA paper 2017–0177, AIAA Scitech Forum*, January 2017. https://doi.org/10.2514/6.2017-0177.

[7] Varigonda, S. V., and Narayanaswamy, V., "Investigation of Shock Wave Oscillations over a Flexible Panel in Supersonic Flows," *AIAA paper 2019–3543, AIAA Aviation Forum*, June 2019. https://doi.org/10.2514/6.2019-3543.

[8] Tan, S. S., Bruce, P. J., and Gramola, M., "Oblique Shockwave Boundary Layer Interaction on a Flexible Surface," *AIAA paper 2019–0097, AIAA Scitech Forum*, January 2019. https://doi.org/10.2514/6.2019-0097.

[9] Spottswood, S. M., Beberniss, T. J., Eason, T. G., Perez, R. A., Donbar, J. M., Ehrhardt, D. A., and Riley, Z. B., "Exploring the response of a thin, flexible panel to shock-turbulent boundary-layer interactions," *Journal of Sound and Vibration*, Vol. 443, 2019, pp. 74–89. https://doi.org/https://doi.org/10.1016/j.jsv.2018.11.035.

[10] Neet, M. C., and Austin, J. M., "Effects of Surface Compliance on Shock Boundary Layer Interaction in the Caltech Mach 4 Ludwieg Tube," *AIAA paper 2020–0816, AIAA SciTech Forum*, January 2020. https://doi.org/10.2514/6.2020-0816.

[11] Schöneich, A. G., Whalen, T. J., Laurence, S. J., Sullivan, B. T., Bodony, D. J., Freydin, M., Dowell, E. H., Stacey, L. J., and Buck, G. M., "Fluid-Thermal-Structural Interactions in Ramp-Induced Shock-Wave Boundary-Layer Interactions at Mach 6," *AIAA paper 2021–0912, AIAA Scitech Forum*, January 2021. https://doi.org/10.2514/6.2021-0912.

[12] Clemens, N. T., and Narayanaswamy, V., "Low-Frequency Unsteadiness of Shock Wave/Turbulent Boundary Layer Interactions," *Annual Review of Fluid Mechanics*, Vol. 46, No. 1, 2014, pp. 469–492. https://doi.org/10.1146/annurev-fluid-010313-141346.

[13] Eitner, M. A., "Experimental Investigation of Fluid-Structure Interaction of a Compliant Panel in Mach 2 Flow under a Compression Ramp Shock-Boundary Layer Interaction," Ph.D. thesis, The University of Texas at Austin, 2021.

[14] Spottswood, S., Eason, T., and Beberniss, T., "Influence of shock-boundary layer interactions on the dynamic response of a flexible panel," *ISMA 2012 International Conference on Noise and Vibration Engineering*, Katholieke Universiteit Leuven Leuven, Belgium, 2012, pp. 603–617.

[15] Ganapathisubramani, B., Clemens, N. T., and Dolling, D. S., "Effects of upstream boundary layer on the unsteadiness of shock-induced separation," *Journal of Fluid Mechanics*, Vol. 585, 2007, p. 369–394. https://doi.org/10.1017/S0022112007006799.

[16] Ganapathisubramani, B., "Statistical properties of streamwise velocity in a supersonic turbulent boundary layer," *Physics of Fluids*, Vol. 19, No. 9, 2007, p. 098108. https://doi.org/10.1063/1.2772303.

[17] Stone, J. V., "Blind Source Separation Using Temporal Predictability," *Neural Computation*, Vol. 13, No. 7, 2001, pp. 1559–1574. https://doi.org/10.1162/089976601750265009.

[18] Olson, M. D., "Some flutter solutions using finite elements," *AIAA Journal*, Vol. 8, No. 4, 1970, pp. 747–752. https://doi.org/10.2514/3.5751.

[19] Dowell, E. H., *Aeroelasticity of plates and shells*, Vol. 1, Springer Science & Business Media, 1974.

[20] Babinsky, H., and Harvey, J. K., *Shock Wave-Boundary-Layer Interactions*, 1st ed., Cambridge Aerospace Series, Cambridge University Press, 2014.